Iranian Journal of Medical Physics

ijmp.mums.ac.ir

Utilization of an optimum low-pass filter during filtered back-projection in the reconstruction of single photon emission computed tomography images of small structures

Mpumelelo Nyathi[1*]

1. Department of Medical Physics, Faculty of Health Sciences, SefakoMakgatho Health Sciences University, Ga-Rankuwa, South Africa

ARTICLE INFO

Article type:
Original Article

Article history:
Received: Dec31, 2017
Accepted: Nov11, 2018

Keywords:
Nuclear Medicine
SPECT
Imaging
Radionuclide Imaging

ABSTRACT

Introduction:Low-pass filters eliminate noise, and accordingly improve the quality of filtered back-projection (FBP) in the reconstruction of single photon emission computed tomography (SPECT) images. This study aimed at selection of an optimum low-pass filter for FBP reconstruction of SPECT images of small structures.

Material and Methods:Spheres A, B, and C (16 mm, 12 mm, and 11 mm in diameter, respectively) attached to capillary stems were filled with technetium-99m solution (activity concentration 300 kBq/mL). They were then mounted inside a Jaszczak Phantom forming a V-shaped structure. The phantom was then filled with distilled water. Two-dimensional (2D) projections were acquired on 128 ×128 pixels using a Siemens E-Cam dual-head gamma camera. The Parzen, Shepp-Logan, Low Pass Cosine filters (cut-off frequencies: 0.2-0.9), and Butterworth filter (order: 1-9; cut-off frequencies: 0.3-0.9) were employed during FBP reconstruction. The line command of ImageJ software was used to draw the point spread functions of acquired 2D transaxial central slices and for the measurement of their full-width at half-maximum (FWHM).

Results:The FWHM of 2D central image slices of spheres A, B, and C reconstructed using a Butterworth filter measured 20, 20, and 10 pixels, respectively. In comparison, the reconstructed images using the Parzen, Low Pass Cosine, and Shepp-Logan filters measured to 27, 25 and, 22 pixels for sphere A, 24, 22, 20 pixels for B, and 22, 20, 18 pixels for C, respectively.

Conclusion: The low-pass filters successfully suppressed noise during the FBP reconstruction of SPECT images of small structures. Accordingly, the Butterworth is a suitable choice.

►*Please cite this article as:*
NyathiM.Utilization of an optimum low-pass filter during filtered back-projection in the reconstruction of single photon emission computed tomography images of small structures.Iran J Med Phys 2019; 16: 300-306.10.22038/ijmp.2018.27777.1297.

Introduction

Nuclear medicine is a diagnostic and therapeutic modality [1]. A radioactive drug is administered in very small amounts into the human body [2] aimed at targeting the investigated organ by the end of its biodistribution. A gamma camera is then used to acquire two dimensional (2D) projections of the distribution of the activity within the targeted organ or tissue under the study [1]. The acquired projections are then reconstructed to give a three-dimensional (3D) view of the targeted organ [1, 3]. Previously, filtered back-projection (FBP) was the most widely used image reconstruction technique. However, with developments in computer technology, the use of algebraic techniques has increased as more robust methods [4].

Despite the increase in the use of iterative techniques [4], the FBP reconstruction technique can still play a significant role in SPECT image reconstruction [5, 6]. However, the drawback of using FBP technique is the amplification of noise on the projections during the reconstruction process resulting in the acquisition of noisy images. The noise is composed of frequencies which do not contain the required patient information. However, it can be eliminated through a mathematical process called image filtering [7-9]. The process involves the use of a ramp filter in conjunction with low-pass filters [9]. A low-pass filter allows the retention of low frequencies unaltered while blocking high frequencies; therefore, it is also referred to as a smoothing filter.

The Parzen, the Hanning, and the Butterworth filters are among the commonly used low-pass filters [7, 9, 10]. Low-pass filters are supplied in the default settings of the gamma camera by the manufacturers without any advice on their selection, which makes filter selection a tedious process. Furthermore, a particular low-pass filter that may be effective for one study may not be suitable to use in other clinical situations. The low-pass filters are generally characterized by either one or two parameters, namely the order and the cut-off frequency. The cut-off frequency defines the bandwidth of the filter, where frequencies higher than the cut-off value are suppressed [4, 11, 12]. The image noise is best

*Corresponding Author: Email:Mpumelelo.Nyathi@smu.ac.za

suppressed by low cut-off filters, compared to high cut-off filters. The low cut-off filters may blur the image, on the other hand, the high cut-off filters are known to preserve the resolution despite their inability to effectively suppress noise [4, 9].

Ramp filter

The ramp filter is a compensatory filter. It is considered as a high pass filter. The compensatory effect of the filter is derived from the fact that it eliminates the star artifact consequences of the simple projection. The ramp filter only allows the passage of high frequencies while restricting the passage of low frequencies. The ramp filter can only be applied in the transaxial plane, where the blurring appears [9]. The ramp filter function in the frequency domain is described by Equation 1 [4].

$$H_R(k_x,k_y)=k=(k_x{}^2+k_y)^{1/2} \quad (1)$$

Where, $k$is the ramp filter frequency, while k_x and k_y are values on a rectangular grid of k-space.

The use of the ramp filter results in an image with sharp edges. However, the main disadvantage of this filter is that it cannot eliminate the noise that was present in 2D image projections and now amplified during the FBP reconstruction process. In order to overcome this limitation, the ramp filter should always be used in conjunction with a low-pass filter aiming at the reduction of the noise [4, 13]. Therefore, the use of a ramp filter in conjunction with a low-pass filter makes it possible to obtain SPECT images reconstructed with FBP technique that is less noisy [4]. However, the challenge is to select a low-pass filter with suitable characteristics capable of eliminating or reducing noise while preserving the spatial resolution.

The Parzen filter

The Parzen filter is a smoothing filter, which can eliminate noise at high frequency. However, it degrades the spatial resolution. The Parzen filter function is defined in the frequency domain by the *Equation 2* [4, 13].

$$|f|-6|f|\times\left(1-\frac{|f|}{f_m}\right)^2\times\left(1-\frac{|f|}{f_m}\right)\left(|f|\pi\frac{f_m}{2}\right),$$

$$P(f)\begin{cases}2|f|\left(1-\frac{|f|}{f_m}\right)^3, & (\frac{f_m}{2}\pi|f|)\,\pi\,0\\ 0, & (|f|\geq f_m),\end{cases} \quad (2)$$

Where, f represents frequency and $f_m$is the critical cut-off frequency.

The Hanning filter

The Hanning filter removes high frequencies among which include the noise. It is characterized by a single parameter (the cut-off frequency).A typical Hanning quickly falls into zero, which makes it effective in noise reduction. However, it does not preserve the edges. A Hann window function is used during signal processing and the process is called "Hanning." The Hanning filter function in frequency domain is defined by the Equation 3 [4]:

$$H(f)=\begin{cases}0.5+0.5\cos\frac{\partial f}{f_m} & 0\leq|f|\leq f\\ 0 & otherwise\end{cases} \quad (3)$$

Where,f denotes the spatial frequency of the image and f_m is the critical cut- off frequency.

The Butterworth Filter

The Butterworth filter is a low-pass filter that is generally preferred in SPECT image filtering. It has the potential of reducing the noise while preserving image resolution [4].It is well suited for utilization due to its ability to change the shape through the cut-off frequency and the order parameter. The speed of the cut-off frequency depends on the order. The ability of the Butterworth filter to change shape makes it easily adaptable to the frequency characteristics of the projection data.

A Butterworth filter function is described by Equation *4* [4].

$$B(f)=\frac{1}{[1+(f/f_C)]^{2n}} \quad (4)$$

Where,f is the spatial frequency domain, $f_C$refers to the critical frequency, and n denotes the order of the filter.

The Shepp-Logan

The Shepp-Logan filter falls under the category of low-pass filters. It is defined by the mathematical *Equation 5* [4].

$$S(f)=\frac{2fm}{[\pi(\sin|f|\pi/2fm)]} \quad (5)$$

Where,*f* represents the frequency of the image and f_m is the critical cut-off frequency.

Components of a SPECT image projection

An acquired SPECT 2D projection consists of a nuclear medicine signal that includes patient information and noise. In this regard, noise is unwanted information that hinders the accurate diagnosis of the patient disease and is uniformly distributed across the spectrum. The noise is amplified during the FBP reconstruction. A ramp filter applied during FBP reconstruction removes the star artifact and the noise in the lower spectrum; however, it leaves noise in the upper section of the spectrum [4, 11]. A low pass filter selected manually by the user for use in conjunction with the ramp filter during the FBP reconstruction can reduce the noise [4, 9, 10]. The low-pass filters allow the retention of the patient information unaltered meanwhile blocking the image noise [5, 8-13]. However, the low-pass filters can degrade the spatial resolution resulting in images with

blurred edges and the need for selecting a low-pass filter with the ability to trade-off between noise reduction and preservation of the spatial resolution.

One of the main goals of filtering is to compensate for the loss of image details by reducing noise. Image filtering greatly improves the quality of a SPECT image yielding information obscured by the presence of noise. This study aimed at the selection of an optimum low-pass filter during FBP reconstruction of SPECT images of small structures.

Materials and Methods

Phantom preparation

Three hollow sphere inserts, namely A, B, and C (with diameters of 16 mm, 12 mm, and 11 mm, respectively), were all attached to capillary stems. They were filled with technetium-99m solution (300 kBq/mL) prior to being mounted inside a BiodexJaszczak SPECT Phantom (Data Spectrum Corporation, United States of America) [2], forming a V-shaped structure with each sphere touching the walls of the phantom. This position helped to maintain the detector head as close as possible to the spherical source in order to improve spatial resolution. The phantom was then filled with distilled water.

Imaging protocol

The phantom was laid horizontally along the axis of the imaging table of the Siemens E-Cam dual-head gamma camera (Siemens Medical Solutions USA, Inc.) fitted with low energy high-resolution collimators (Figure 1). The energy window of the Siemens E-Cam dual-head gamma camera was fixed at 140 keV$\pm$15% photo peak. This energy window proved effective in the rejection of Compton scatter photons.

Figure 1. Acquisition of 2D projections of the phantom using a Siemens E-cam dual-head gamma camera

The matrix size of 128×128 pixels was selected for SPECT imaging. This matrix size gives a good trade-off between the improvement in the spatial resolution and image degradation by the noise when a concentration of 300 kBq/mL is used during imaging [2]. With magnification set to one (1.0), a non-circular orbit actioned automatically during the acquisition of 2D projections over a duration of 30 minutes.

Image reconstruction

Image reconstruction was performed using the FBP technique and windowing was performed with each of the low-pass filters independently (i.e., the Butterworth, the Parzen, the Shepp-Logan, and the Low Pass Cosine). The values of the cut-off frequency for the Parzen, the Shepp-Logan, and the Low Pass Cosine were blindly selected to evenly cover the whole range of variables in steps of 0.1 within the range of 0.2-0.9. A total of 21 filtering combinations were considered. The cut-off frequencies for the Butterworth filter were selected to cover a range of 0.30-0.9 in steps of 0.1. For each chosen cut-off frequency, the order of the Butterworth was selected to cover a range of 1-9 in steps of 1 unit for each reconstruction performance. A total of 7 combinations of orders and cut-off frequencies were used in this study.

Measurement of the full-width at half-maximum of the 2D transaxial central image slices of spheres A, B, and C

A point spread function (PSF) for each 2D central image slices corresponding to the spheres A, B, and C was reconstructed using FBP process with the line command tool of ImageJ software (version 1.48a; Java 1.70_51 [64-bit]) [2]. In the next step, the FWHM corresponding to the PSF was measured in pixels with the line command of ImageJ software. The FWHMvalues represented the spatial resolution for the central slices of the spheres A, B and C.

Results

Window function of the Parzen, Shepp-Logan, and Low Pass Cosine filters

Figure 2 shows the variation of the FWHM of the 2D transaxial central image slice of sphere A with the cut-off frequency. As can be seen in Figure 2, a dramatic improvement of the spatial resolution is observed as the cut-off frequency increased from 0.7 to 0.9 with the implementation of the Parzen filter. However, the implementation of the Low Pass Cosine filter indicated that the measured FWHM values started to improve at a cut-off frequency of 0.6 reaching the value of 25 pixels at a cut-off frequency of 0.9, compared to 27 pixels measured for the Parzen filter at the same cut-off frequency. However, the implementation of the Shepp-Logan filter showed that the spatial resolution started to improve at a much lower cut-off frequency of 0.5 yielding the best value of the measured FWHM (22 pixels) at a cut-off frequency of 0.9.

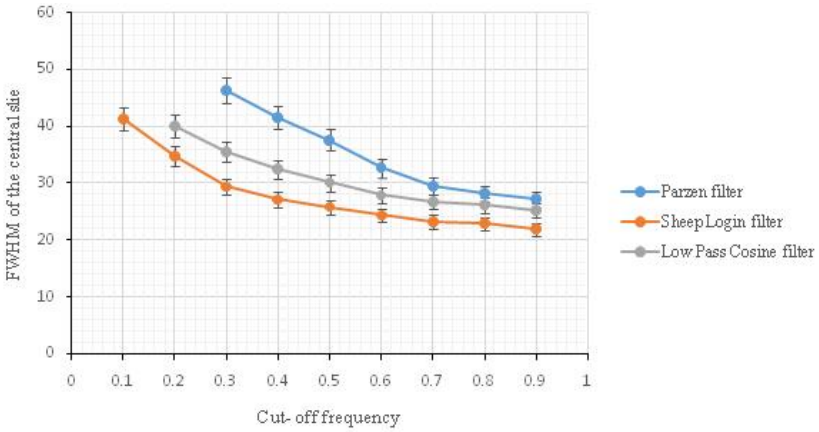

Figure 2. Variation of the FWHM for the 2D central slice of sphere *A* with the increase of the cut-off frequency

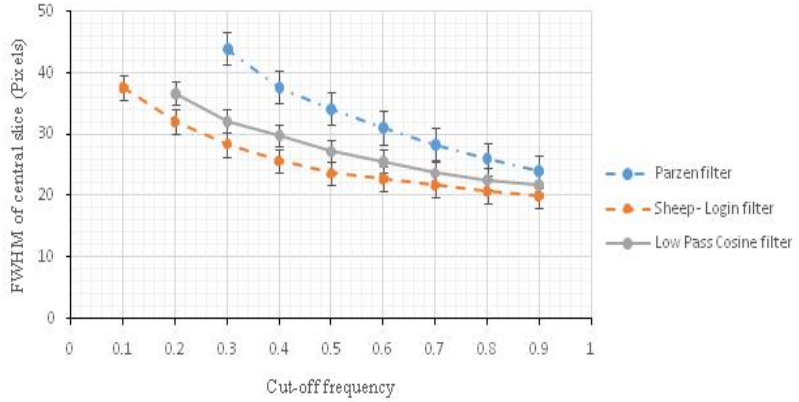

Figure 3. Variation of the FWHM for the 2D transaxial central slice of sphere *B* with the increase of the cut-off frequency

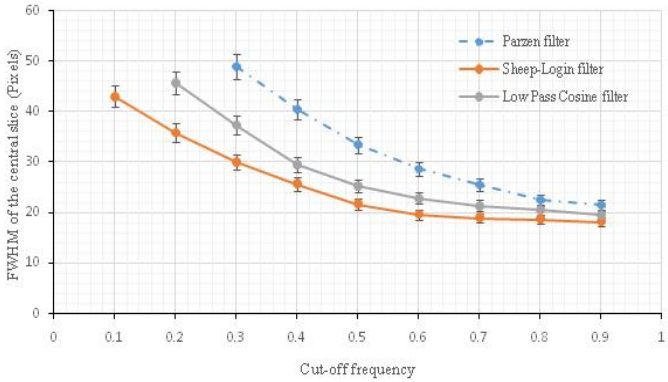

Figure 4. Variation of the FWHM for the 2D central slice of sphere *C* with the increase of cut-off frequency

The improvement in the FWHM of the 2D transaxial central image slice of sphereB was similar to that of the 2D transaxial central image slice of sphere A whenwindowing was performed using the Parzen, Low Pass Cosine and Shepp-Logan. However, obtained values of the FWHM (24, 22, and 20 pixels) were better for the2D transaxial image slice through the implementation of the Parzen, the Low Pass Cosine, and the Shepp-Logan, respectively, compared to sphere A at a cut-off frequency of 0.9 (27, 25, and 22 pixels; Figure 3).

Figure 4 shows the variation of the FWHM for the 2D transaxial central slice of sphere Cwith the increase of the cut-off frequency reconstructed through the independent implementation of the Parzen, Low Pass Cosine, and Shepp-Logan in conjunction with the ramp filter during the FBP reconstruction process.

As Figure 4 shows, it can be observed that the values of the FWHM elevated at cut-off frequency of 0.5 reaching to the best value at of 0.9. The best-measured values of the FWHM (i.e., 22, 20, and 18 pixels) were achieved through the implementation of the Parzen, Shepp – Logan, and Low Pass Cosine filters, respectively at a cut-off frequency of 0.9.

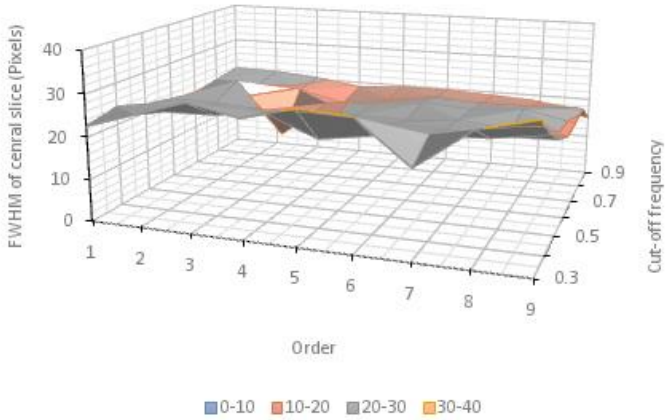

Figure 5. Variation of the FWHM of the 2D central slice of sphere *A* with the increase of order and the cut-off frequency

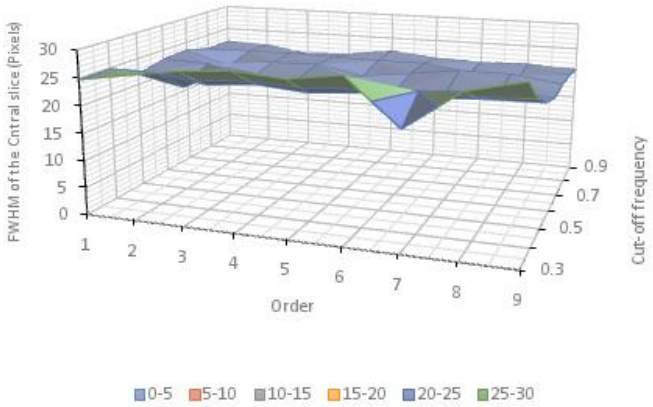

Figure 6. Variation of the FWHM of the 2D central slice of sphere *B* with the increase of order and the cut-off frequency

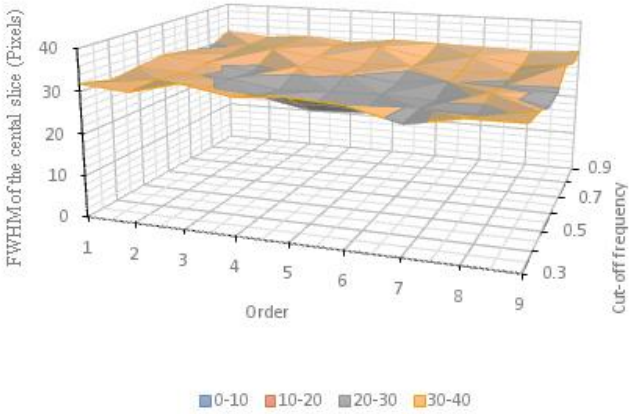

Figure 7. Variation of the FWHM of the 2D central slice of sphere *C* with the increase of order and the cut-off frequency

Window function of the Butterworth filter

The measured value of FWHM for the 2D transaxial central slice of sphere A did not change significantly as the order was varied for a fixed cut-off frequency, which leads to the best-obtained value of 20 pixels (Figure 5). A similar value was achieved for the 2D transaxial central image slice of sphere B (Figure 6). However, significant changes were observed in the 2D transaxial central image slice of sphere C, which resulted in the best-measured FWHM value of 10 pixels (Figure 7).

Discussion

The SPECT is a diagnostic functional imaging modality [5], which can detect the slight changes in the physiological processes taking place inside the organ before any structural changes can be observed. Information on the regional tissue function may also be obtained using the SPECT imaging modality [14]. These properties make SPECT more helpful compared to the high-resolution imaging modalities, such as computed tomography and magnetic resonance imaging. The SPECT images makes it possible to detect changes in the function of the organ before any structural changes can be observed. The SPECT imaging is renowned for

its role in quantitative evaluation of the cardiac function as well as evaluation of the tumor volume [13].

Its ability to determine tumor volume as well as quantifying radioactivity uptake within a tumor is important when monitoring tumor's response to therapy. However, this can only be achieved if accurate quantitative values are obtained from the SPECT images of tumors or diseased organs. Clinicians can use the accurate quantitative values of the SPECT images to determine the patients' needs to continue the therapy or withdraw from the treatment. However, the ability to obtain accurate quantitative values depends on the quality of the obtained SPECT images of the tumors. Image quality may be degraded due to the limited resolution of the gamma camera imaging system and the need to acquire images with good quality in order to achieve the desired clinical objectives. In order to guarantee good resolution, the SPECT images of spheres A, B, and C were acquired on a matrix size of 128×128 pixels. In a study conducted by Mpumelelo [2], this matrix size was found to be ideal for the acquisition of images with diameters two-three times less than the resolution of the gamma camera since it trades trade-off between the improvement in the spatial resolution and reduction of image noise inherent to low photon count on the acquired images (images of spheres A, B, and C in our case had dimensions in that range). A trade-off in improvement of the spatial resolution and noise is crucial since these two image degrading factors are intertwined [2].

The image noise impairs the visualization of the desired important image data required to make accurate visual or quantitative interpretation in order to achieve an accurate diagnosis [4]. Despite using the matrix size of 128×128 pixels which maintained a balance between improvement in the spatial resolution and reduction of the noise produced through the 2D projections of the spheres [2], the reconstructed SPECT images were bound to remain degraded by noise due to their reconstruction using FPB reconstruction process. During FPB reconstruction, the noise originating from the acquired 2D projections is amplified [3, 4]. Therefore, the noise after FBP reconstruction remains a cause of concern since it consists of high-frequency data and at the same time the image data linked to the edges of the image also contains high frequencies. In order to eliminate the high frequencies in image noise, it is recommended to use the low pass filters [3] which improves the spatial resolution recovery while suppressing the noise [4, 11].

In this study, the low-pass filters (the Butterworth, the Parzen, the Shepp-Logan, and the Low Pass Cosine) were successfully used to suppress noise while preserving the resolution of the images of the small structures (spheres A, B, and C). As can be seen in figures 2, 3, and 4, the Shepp-Logan offered a better compromise between the image noise reduction and the resolution recovery compared to the Parzen and the Low Pass Cosine filters during the FBP image reconstruction of spheres A, B, and C (with the diameters of 16 mm, 12 mm, and 11mm, respectively). The study also revealed that as the cut-off frequency was elevated, the resolution recovery improved up to a cut-off frequency of 0.9. This cut-off frequency (i.e., 0.9) offered a good trade-off between image noise suppression and resolution recovery.

In addition, figures 2, 3, and 4, show that the Shepp-Logan filter offers the best spatial resolution compared to the Parzen and the Low Pass Cosine filters. However, Maria et al. [15] mentioned that the use of Shepp-Logan offers images of the highest resolution with least smoothing compared to the images reconstructed using the Parzen filter. The Sheep-Login, is suitable for the reconstruction of SPECT images of small tumors, used for visual interpretation or qualitative assessment to determine the response to radiation therapy.

In order to choose an optimum filter, the contrast and signal noise-to-ratio (SNR) also plays a significant role particularly for qualitative analysis [9, 16]. Dong et al. [16] found that the minimum values of contrast would lead to the decreased level of tumor visibility. Accordingly, the use of the Sheep-Logan would result in better visibility compared to use of the Parzen filter where qualitative analysis is a priority. These findings were in agreement with results of our study in which among the three spheres A, B and C, the Shepp-Logan offered best spatial resolution (figures 2, 3, and 4). Although the Parzen filter does not offer good resolution recovery (figures 2, 3, and 4), it can still be helpful for quantitative studies since the edges of the image may not be important for such studies. Yusoff and Zakaria [9] suggested that the Parzen filter is the best for detecting the defect size in myocardial SPECT imaging.

A study conducted by Dong et al. [16] revealed that the SNR attributed to the Shepp-Logan was equally comparable to that of the Parzen filter. However, it was lower compared to the SNR value for Butterworth filter. Furthermore, they also found that the Butterworth filter exhibited highest contrast and a little low level of noise compared to the other two filters.

According to the obtained results of the current study, it was found that among the low pass filters (the Parzen, Shepp-Logan, Low Pass Cosine, and the Butterworth), the application of the Butterworth filter during the FBP reconstruction for the images of spheres A, B, and C improved the values of the FWHW (20, 20, and 10 pixels), respectively as illustrated in figures 5, 6, and 7. Therefore, the Butterworth filter proved to be the best of all the low-pass filters in resolution recovery. The advantage of the Butterworth filter relied on of its ability to change its shape to adapt to the characteristics of the projection data using the parameter order. As a result, it enables the cut-off frequency to quickly role to zero without removing the high-frequency data that constitutes the edges of the image.

Yusoff and Zakaria reported that the Butterworth filter can maintain a balance between image quality and size accuracy [9]; therefore, its use is recommended when reconstructed images are required for quantitative analysis. Moreover, Dong et al. pointed that the further

advantage of the Butterworth filter is its ability to keep a balance between the needs of high contrast and low noise [16]. Another study by Groch and Erwin [12] indicated that the Butterworth filter was the best low-pass filter for use in ^{99m}Tc-HMPAO brain SPECT as it gave the best compromise between noise elimination and spatial resolution recovery in comparison to the Hanning filter. However, the parameters for all studies involving the use of the Butterworth filter differed depending on the type of study. For example, in a study conducted by Zaidi [17], the cut-off frequency was equivalent to 04 N and an order 3 were used for the reconstruction of transaxial slices with the thickness of 1 pixel during quantifying thyroid volume by SPECT. These variations demonstrate that the Butterworth filter must be standardized for a particular study. The obtained results of these studies were in line with our findings, meaning that the parameters of the Butterworth filter are dependent on the size of structure being imaged, and accordingly we obtained different parameters for the spheres A, B, and C.

Conclusion

The study established that low-pass filters (the Parzen, Shepp-Logan, Low Pass Cosine, and the Butterworth) can successfully suppress noise during the FBP reconstruction of 2D image projections of small structures (diameters 11mm, 12 mm, and 16mm). The Butterworth filter produced the best spatial resolution, and accordingly it can be used where there is need to trade-off between the preservation of the spatial resolution and reduction of noise during FBP reconstruction of images of small structures. Lastly, the choice of the low-pass filter depends on the type of study and the size of organ or structure under the study and it still remains a challenge in SPECT image reconstruction.

Acknowledgment

The author wishes to acknowledge Dr George Mukhari Academic Hospital, South Africa for availing the gamma camera used in this study.

References

1. Zaidi H. Quantitative Analysis in Nuclear Medicine Imaging. Boston, MA: Springer Science & Business Media, Inc. 2006.
2. Mpumelelo N. Determination of Optimum Planar Imaging Parameters for Small Structures with Diameters Less Than the Resolution of the Gamma Camera. Iran J Med Phys. 2017; 14219-28. DOI: 10.22038/ijmp.2017.24559.1246.
3. Lyra M, Ploussi A, Rouchota M, Synefia S. Filters in 2D and 3D Cardiac SPECT Image Processing. Cardiol Res Pract. 2014; 2014:963264. DOI: 10.1155/2014/963264.
4. Lyra M, Ploussi A. Filtering in SPECT Image Reconstruction. International Journal of Biomedical Imaging. 1; 2011:10. DOI: 10.1155/2011/693795.
5. Sayed IS, Nasrudin NSM. Effect of Cut-Off Frequency of Butterworth Filter on Detectability and Contrast of Hot and Cold Regions in Tc-99m SPECT. International Journal of Medical Physics, Clinical Engineering and Radiation Oncology. 2016; 5: 100-9.
6. Zeng GL. Revisit of the Ramp Filter. IEEE Trans Nucl Sci. 2015; 62(1): 131‑6. DOI:10.1109/TNS.2014.2363776.
7. Mettler Jr FA, Guiberteau MJ. Essentials of Nuclear Medicine Imaging. 4th ed. Philadelphia; Saunder an Imprint of Elservier; 2003.
8. Sadremomtaz A, Taherparvar P. Filtering in SPECT Image Reconstruction The influence of filters on the SPECT image of Carlson phantom. J. Biomedical Science and Engineering. 2013; 6: 291-7.
9. Yusoff M, Salihin N, Zakaria A. Determination of the optimum filter for qualitative and quantitative 99mTc myocardial SPECT imaging. Iran J Radiat Res. 2009; 6:173-82.
10. Benjamin G, Tsui MW, McCartney W, Perry J, Berg J. Determination of the Optimum Filter Function for SPECT Imaging. J Nucl Med. 1988; 29:643-50.
11. Hawkings J. The basics of tomographic Reconstruction and filtering. 2017 [cited 2017 Oct 10]: Available from: http://passthrough.fw-notify.net.
12. Groch MW, Erwin WD. SPECT in the year 2000: Basic Principles. J Nucl Med. 2000; 28: 233-44.
13. Links J.M, Advances in nuclear medicine instrumentation: considerations in the design and selection of an imaging system. Eur J Nucl Med. 1998; 25:10.
14. Livieratos L. Basic Principles of SPECT and PET imaging. Chapter 12. Radionuclide and Hybrid Bone Imaging. Springer-Verlag Berlin Heidelberg. 2013.
15. Maria LG, Agapi P, Maritina R, Stella S. Filters in 2D and 3D Cardiac SPECT Image Processing. 2018 [cited 2018 Nov 8]. Available from: http://avidscience.com.
16. Dong X, Saripan MI, MahumudR, Mashohor S, Wang A. Determination of the optimum filter for 99mTc SPECT breast imaging using a wire mesh collimator. Pak J Nucl Med. 2017; 7(1):9-15.
17. Zaidi H. Comparative methods for quantifying thyroid volume using planar imaging and SPECT. Journal of Nuclear Medicine. 1996; 37 (8):1421‑2.